# An improved routing algorithm for a large-scale distributed hydrological model with consideration of underlying surface impact

Jingjing Li, Haoyuan Zhao, Jun Zhang, Hua Chen, Chong-Yu Xu **IWA**, Lu Li, Jie Chen and Shenglian Guo

## ABSTRACT

Large-scale hydrological models are important tools for simulating the hydrological effect of climate change. As an indispensable part of the application of distributed hydrological models, large-scale flow routing methods can simulate not only the discharge at the outlet but also the temporal and spatial distribution of flow. The aggregated network-response function (NRF), as a scale-independent routing method, has been tested in many basins and demonstrated to have good runoff simulation performance. However, it had a poor performance and produced an unreasonable travel time when it was applied to certain basins due to a lack of consideration of the influence of the underlying surface. In this study, we improve the NRF routing method by combining it with a velocity function using a new routing parameter $b$ to reflect the wave velocity's sensitivity to slope. The proposed method was tested in 15 catchments at the Yangtze River basin. The results show that it can provide better daily runoff simulation performance than the original routing model and the calibrated travel times in all catchments are more reasonable. Therefore, our proposed routing method is effective and has great potential to be applied to other basins.

**Key words** | DEM-based routing method, distributed hydrological model, NRF routing method, velocity function, WASMOD, Yangtze River basin

**Jingjing Li**
**Haoyuan Zhao**
**Hua Chen** (corresponding author)
**Jie Chen**
**Shenglian Guo**
State Key Laboratory of Water Resources and
    Hydropower Engineering Science,
Wuhan University,
Wuhan,
China
E-mail: chua@whu.edu.cn

**Jun Zhang**
Bureau of Hydrology,
Changjiang Water Resources Commission,
Wuhan,
China

**Chong-Yu Xu** IWA
Department of Geosciences,
University of Oslo,
Oslo,
Norway

**Lu Li**
NORCE Norwegian Research Centre, Bjerknes
    Centre for Climate Research,
Jahnebakken 5, 5007 Bergen,
Norway

## HIGHLIGHTS

- This study coupled the aggregated network-response function (NRF) flow routing method with a velocity function.
- The improved NRF method reflects the sensitive wave velocity to slope and gets better runoff simulation performance.
- The calibrated travel time is closer to benchmark value after improvement.
- The improved NRF method adapts to basins of various underlying surfaces.
- The improved NRF method gets more reasonable wave velocity after improvement.

## INTRODUCTION

Climate change has received widespread attention from the scientific community and the public, as it has caused a series of serious problems, including natural disasters and extreme climate events (Kharin *et al.* 2018; Chen *et al.* 2019; Lu & Qin 2020; Ragettli *et al.* 2020). As tools for estimating regional and global water resources and predicting the hydrological response to climate change, large-scale hydrological models have become a hot topic recently (Müller Schmied & Döll 2017; Wang *et al.* 2018; Abou Rafee *et al.* 2019; Li *et al.* 2019). A large-scale routing method is an important part of a large-scale hydrological model, with which a distributed hydrological model can simulate the change in runoff at temporal and spatial scales (Beven 2001). Many routing methods based on a digital elevation model (DEM) have been developed (Wen *et al.* 2012; Li *et al.* 2014; Lu *et al.* 2015; Huang & Lee 2017; Ling *et al.* 2018; Fan *et al.* 2019). The main steps of runoff routing in distributed hydrological models are (1) extracting the flow network and (2) calculating the runoff routing according to the flow path (Wen *et al.* 2012). Generally, runoff routing based on a DEM is calculated in one of two ways (Olivera *et al.* 2000): cell-to-cell and source-to-sink. The cell-to-cell method calculates the water movements from each grid to its adjacent downstream grid until the outlet grid of the basin is reached. The outflow of each cell is calculated based on the inflow and the river channel's storage. The source-to-sink method, under the assumption that the water is rigid, directly calculates the water's movement from the grid where runoff is generated to the outlet of the basin.

The first of these two kinds of routing methods is based on the mass conservation equation and the channel storage function equation. It is widely used due to its simplicity (Miller *et al.* 1994; Sausen *et al.* 1994; Arora & Boer 1999; Huang & Lee 2017). In addition to its simplicity, the cell-to-cell routing method has other advantages. It has the potential to include the nonlinear losses from the surface water to the groundwater because it considers the feedback between the flow and the water storage in each cell (Naden *et al.* 1999). Besides this, with the cell-to-cell routing method, the water storage in any cell of interest can be queried at each time step. If the ratio of land area covered by surface

water to the total land area can be calculated based on the water storage in each cell, it will contribute to land–atmosphere interaction simulation (Olivera *et al.* 2000). However, the choice of a proper spatial resolution is a dilemma for the cell-to-cell routing method. In distributed hydrological models, high resolution can reflect the heterogeneity of the hydrological characteristics of the basin and improve the accuracy of calibrated parameters. On the other hand, higher-resolution DEM will lead to a significant increase in the amount of required computations, especially when coupled with a meteorological model because the meteorological model has vast computational cost. However, a coarser resolution may lead to a decrease in model performance due to not considering routing within the cell (Arora *et al.* 2001; Gong *et al.* 2009). Besides this, there may be a great difference between the network that is generated at a coarse resolution and the true one, which is another disadvantage of the cell-to-cell routing method. Attempts have been made to bring a network that is generated at a coarse resolution closer to the real one. However, a gap still exists (Fekete *et al.* 2001; Guo *et al.* 2004).

Some of the source-to-sink routing methods have the same disadvantages as the cell-to-cell method, including the routing models by Ducharne *et al.* (2003) and Guo *et al.* (2004), which will provide worse performance as the cell resolution becomes coarser. The routing model by Ducharne *et al.* (2003) uses the mean travel time of each large routing cell, so the water in a cell will arrive at the outlet in the same day. This can be unreasonable, especially when the cell size is large. The routing model by Guo *et al.* (2004) uses the mean flow path length for each cell, making the routing method scale-dependent. Therefore, it would benefit a hydrological modeler to find a routing method with the capability to be scale-independent, which will preserve the spatially distributed travel time information from a finer-resolution DEM for coarser resolution cells in the large-scale hydrological model. The disadvantages of some source-to-sink routing methods have been overcome by some model developers. For instance, Wen *et al.* (2012) proposed a multiscale routing framework that can reduce the impact of the spatial scale by using histograms for the flow

path lengths. The aggregated network-response function (NRF) routing method (Gong *et al.* 2009) can preserve all of the spatially distributed travel time information in high-resolution Hydro1 k DEM data for cells with different resolutions by aggregating the pixel-response function to the cell-response function (CRF). Thus, NRF has the unique advantage of being able to obtain a stable result when moving from a finer to a coarser resolution, making it a preferable routing method for large-scale hydrological models. Another advantage of source-to-sink methods is the computation efficiency (Naden *et al.* 1999; Olivera *et al.* 2000; Gong *et al.* 2009), which enables them to be widely applied (Olivera *et al.* 2000; Ducharne *et al.* 2003; Gong *et al.* 2011; Lu *et al.* 2015).

NRF, as a source-to-sink routing method, has been applied in basins of China, North America, and Africa (Gong *et al.* 2009, 2011; Li *et al.* 2010, 2013, 2014; Ngongondo *et al.* 2013). The results showed that NRF provides good daily runoff simulation performance. However, in some cases, the calibrated wave velocity is too large to be physically realistic, and NRF will fail to provide good daily runoff simulation performance if the wave velocity becomes smaller (Gong *et al.* 2011; Li *et al.* 2014). In this method, the underlying factors that affect the routing process are not comprehensively considered. In this respect, the NRF routing method needs to be improved.

This study aims to improve NRF by considering the influence of the underlying surface in order to obtain a more reasonable wave velocity and travel time and better daily runoff simulation performance. To achieve this aim, the original NRF routing method is coupled with a velocity function proposed by Sircar *et al.* (1991) in order to take the underlying surface's influence into consideration, in which a new routing parameter $b$ is added to reflect how sensitive the wave velocity is to slope. The remainder of this paper is organized as follows. Following a description of the study area, we present the original and improved NRF routing methods. Then, the results of a daily runoff and peak flow simulation by the model before and after the improvement are compared. The travel time and routing parameters and the factors that influence them are analyzed and compared in different catchments to explore the relationship between catchment characteristics and model parameters. Finally, we present our conclusions.

## STUDY AREA AND DATA

### Study area

The study area is the Yangtze River basin (24°27′–35°54′ N, 90°33′–122°19′ E). It has a drainage area of 1,800,000 km². As shown in Figure 1, the Yangtze River is the longest river in China and the third longest river in the world. It has a total length of 6,397 km.

The climate, terrain, land cover and land use, and runoff characteristics vary greatly among the catchments in the Yangtze River basin. Fifteen catchments in the Yangtze River basin were selected in this study in order to evaluate the performance of the improved routing method over a wide range of representative catchments. The characteristics of the terrain in those catchments are shown in Table 1. 'Elevation difference' means the height difference between the highest point and the lowest point in a catchment. Table 1 also presents the shape factor and the river length of the catchments. The basin shape factor (Morisawa 1958) is the ratio of the actual basin length to the perimeter of a circle whose area is the same as that of the basin, and measures the general runoff concentration behavior of the basin. Only the first-order stream, second-order stream, and third-order stream (Wang *et al.* 2019) were included in the stream length in this study. A drainage map of the river system and drainage stations can be found in Figure 1.

The Yangtze River basin has very complex terrain, as it flows through mountains, plateaus, hills, and plains. The overall distribution of elevation at the Yangtze River is high in the west and low in the east. The mean elevation of the source of the Yangtze River, which is located in the hinterland of the Qinghai–Tibet Plateau, is more than 4,000 m above sea level (a.s.l.). The middle reaches lie mostly in low mountains areas and the downstream lies mostly in a hilly plain area.

The mean annual precipitation is 1,110 mm. Due to the vast amount of territory, the complex terrain, and the typical monsoon climate, the spatial distribution and the temporal distribution of annual precipitation in the Yangtze River are very uneven (Xu *et al.* 2008). The main source of river runoff in the basin is the rainfall, but snowmelt and groundwater are also important sources of runoff in the upper reaches of the Yangtze River basin (Yao *et al.* 2014). The
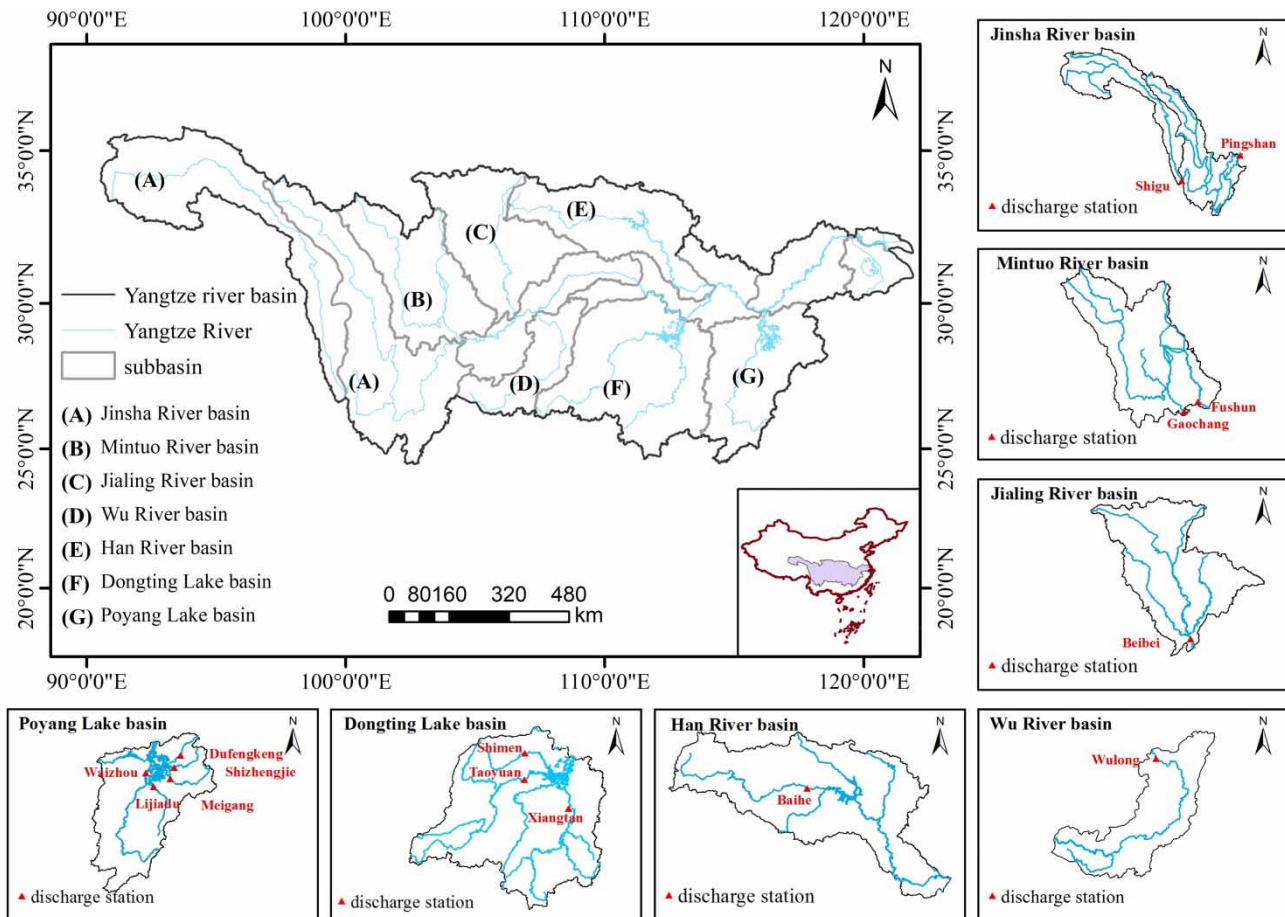
**Figure 1** │ Location of the sub-basins and discharge stations in the Yangtze River basin.

annual mean air temperature in the Yangtze River basin is generally high in the east, low in the west, high in the south, and low in the north. The source area of the basin experiences the lowest temperatures (Su *et al.* 2006).

It is of great significance to simulate the runoff in the Yangtze River basin, as it accounts for 18% of the total area of China, and has more than 400 million people living in it. The Yangtze River basin is also the most important agricultural production base in China because of its warm and humid climate, which provides good conditions for crop growth (Tian *et al.* 2011).

### Data and processing

Hydro1 K (USGS 2001) was used in this study to delineate the basin's boundary. It is a global DEM with a resolution of 1 × 1 km and was produced by the United States

Geological Survey's Earth Resources Observing System. The projection of HYDRO1 k is Lambert azimuthal equal-area projection, whose transformation equations (Weisstein) enable each grid to have an equal area.

Flow direction and flow accumulation databases based on Hydro1 k are also available, which can be used with the discharge stations to obtain the basin's boundary. Then, the estimated basin boundary can be evaluated and corrected based on the basin boundary that was delineated using the finer DEM at the resolution of 90 × 90 m.

Daily precipitation, temperature, and relative humidity data for the period 1969–2008 were taken from the daily dataset of surface climatological data of China (V 3.0) in National Meteorological Information Center (http://data.cma.cn/data/cdcdetail/dataCode/SURF_CLI_CHN_MUL_DAY_V3.0.html). The meteorological data were interpolated using the inverse distance weighted method (Shepard 1968) to be

**Table 1** | Characteristics of the study area

| Sub-basin | River | Station | Mean discharge (m³/s) | Area (km²) | Shape factor | Slope | Mean elevation (m) | Elevation difference (m) | River length (km) |
|---|---|---|---|---|---|---|---|---|---|
| Jinsha River basin | Downstream of Shigu | Pingshan | 4,394.49 | 252,217 | 3.10 | 7.45 | 3,042 | 5,620 | 5,430 |
| | Upstream of Shigu | Shigu | 1,275.61 | 213,003 | 3.66 | 4.87 | 4,569 | 4,124 | 3,559 |
| Mintuo River basin | Tuojiang | Fushun | 360.91 | 23,096 | 2.39 | 1.98 | 590 | 4,523 | 724 |
| | Minjiang | Gaochang | 2,750.02 | 134,622 | 2.47 | 8.88 | 2,949 | 7,087 | 2,924 |
| Jialing River basin | Jialing River | Beibei | 1,841.34 | 157,478 | 2.44 | 6.29 | 1,148 | 2,948 | 3,124 |
| Wu River basin | Wujiang | Wulong | 1,415.63 | 80,099 | 2.71 | 3.91 | 1,104 | 2,628 | 1,237 |
| Han River basin | Hanjiang | Baihe | 686.30 | 54,085 | 2.06 | 6.29 | 1,148 | 2,948 | 1,462 |
| Dongting Lake basin | Xiangjiang | Xiangtan | 1,990.02 | 78,659 | 2.19 | 3.02 | 338 | 1,857 | 2,200 |
| | Yuanjiang | Taoyuan | 2,028.19 | 86,172 | 2.55 | 3.32 | 622 | 2,378 | 2,210 |
| | Lishui | Shimen | 456.86 | 15,118 | 1.96 | 5.12 | 722 | 2,204 | 332 |
| Poyang Lake basin | Gangjiagn | Waizhou | 2,032.18 | 83,532 | 2.27 | 2.46 | 287 | 2,026 | 1,454 |
| | Fuhe | Lijiadu | 376.80 | 16,023 | 2.04 | 2.33 | 227 | 1,415 | 432 |
| | Xinjiang | Meigang | 557.69 | 15,592 | 2.08 | 3.17 | 279 | 2,040 | 323 |
| | Leanhe | Shizhenjie | 296.61 | 8,294 | 1.78 | 2.74 | 205 | 1,421 | 224 |
| | Changhe | Dufengkeng | 155.62 | 4,938 | 1.73 | 3.01 | 246 | 1,361 | 156 |

gridded data, which were used to drive the hydrological model at resolutions of 3, and 10 arc-minutes in the study. The observed daily discharge during 1964–2008 of all catchments, which was used to calibrate and validate the model, was provided by the Bureau of Hydrology of the Changjiang Water Resources Commission.

The travel time of a flood between major hydrological stations in the Yangtze River basin was taken from Zhang *et al.* (2006), which was calculated based on a great deal of data and some proven methods. In this study, it was used as a benchmark to compare the travel time calculated by the original routing method with the travel time calculated by the improved routing method.

## METHODS

### Water and Snow Balance Modeling

The Water and Snow Balance Modeling (WASMOD) system is a conceptual modeling system that was developed by Xu (2002). Different versions of WASMOD have been used in different regions of the world (Widén-Nilsson *et al.* 2007; Gong *et al.* 2011; Kizza *et al.* 2011; Li *et al.* 2011; Yang *et al.* 2018, 2019, 2020). In this study, the daily version of WASMOD was used as a runoff-generation model. As

described in Gong *et al.* (2009), the main components of WASMOD are the computation of snow accumulation and melting, evapotranspiration, slow flow, fast flow, and the total runoff. Compared with the equations in Gong *et al.* (2009), we set two more parameters in this study: $c_5$ is set to correct the precipitation bias, which results from the lack of snow measurements; $c_4$ is set in the potential evaporation equation. As shown in Table 2, there are five to seven parameters with or without the snow module. The snow modules are only applied to Jialing River, Jingsha River, and Mintuo River where snowmelting is one of the most important sources of runoff. If the snow module is not taken into consideration, parameters $a_1$ and $a_2$ will not be

**Table 2** | The parameters of the runoff-generation model and their prior range for calibration

| Parameter | About | Prior range for calibration |
|---|---|---|
| $a_1$ (°C) | Snowfall | [0 to 6] |
| $a_2$ (°C) | Snowmelt | [−6 to 0] |
| $a_4$ (–) | Actual evaporation | [0.1 to 0.999] |
| $c_1$ (1/mm) | Fast runoff | [0 to 0.1] |
| $c_2$ (1/mm) | Slow runoff | [0 to 0.1] |
| $c_4$ (mm day⁻¹ °C⁻²) | Potential evaporation | [$6 \times 10^{-6}$ to $6 \times 10^{-5}$] |
| $c_5$ (–) | Precipitation | [0.5 to 1.5] |

calibrated in the hydrological model.

$$p_t = c_5^* p_{td} \tag{1}$$

where $p_{td}$ is precipitation data described in the Study area and data section and $p_t$ is the corrected precipitation.

$$\text{pet}_t = c_4 \cdot (\max(\text{tmp}_t + 25, 0))^2 \cdot (100 - \text{rh}_t) \tag{2}$$

where $\text{pet}_t$ is the potential evaporation, $\text{tmp}_t$ is the temperature, and $\text{rh}_t$ is the relative humidity.

## The original routing method

Gong *et al.* (2009) developed a routing method, named the aggregated NRF, which was developed with the source-to-sink concept. It builds the relationship between each grid in DEM and the outlet grid.

There are five steps in the improved NRF routing method: (1) extract the flow direction and flow net based on DEM; (2) calculate the travel time $t_i$ between each grid and the outlet of the basin according to the flow path; (3) construct the pixel-response function (PRF) based on $t_i$; (4) calculate CRF based on PRF with the way of linear averaging method; and (5) calculate the discharge at the outlet of the basin based on the result of the runoff-generation model and CRF. The main advantage of NRF is that the routing accuracy is independent of cell size, because the CRF in NRF is not affected by the cell size (Gong *et al.* 2009).

For the wave velocity in grid, Beven & Kirkby (1979) proposed that the overland flow velocity could be calculated based on the topography as follows:

$$v_i = v_{45} \cdot \tan(c_i) \tag{3}$$

where $v_i$ is the wave velocity of the grid, and $c_i$ is the slope of the grid. $v_{45}$ is the wave velocity in the grid whose slope is 45°.

In the study of Gong *et al.* (2009), the authors calculate the wave velocity as follows:

$$v_i = v_{45} \cdot \sqrt{\tan(c_i)} \tag{4}$$

For a given grid, the travel time can be calculated as follows:

$$t_i = \begin{cases} \sum_{i=1}^{k} \dfrac{l_i}{v_{45} \cdot (\tan(c_i))^{0.5}} & c_i > c_0 \\ \sum_{i=1}^{k} \dfrac{l_i}{v_{45} \cdot (\tan(c_0))^{0.5}} & c_i \le c_0 \end{cases} \tag{5}$$

where $c_i$ is the slope, $v_i$ is the wave velocity, $t_i$ is the travel time of the grid, $c_0$ is the slope threshold, which is set to be a constant to prevent $t_i$ from being infinite, and $k$ is the number of grids through the flow path. The slope threshold is 0.1 in this study.

Other details about the NRF routing methods can be seen in Gong *et al.* (2009). In this study, the computation cell size in each catchment was determined by its area to ensure a modest number of cells. The cell size in a larger catchment is larger. Conversely, the cell size is smaller in a smaller catchment. The cell size was set to be $10'$ at catchments whose area is greater than 50,000 km². It was set to be $3'$ at catchments whose area is less than 10,000 km² and $6'$ otherwise.

## The improved routing method

The NRF routing method performed well in the Dongjiang basin and the Willamette basin; however, the calibrated parameter ($v_{45}$) in the Hydro1 k-driven NRF routing method showed an unrealistic value (greater than 25 m/s) (Gong *et al.* 2009, 2011). To improve the NRF, we combine the original routing method with a wave function given by Sircar *et al.* (1991) and modified the equation as:

$$v_i = v_{45} \cdot (\tan(c_i))^b \tag{6}$$

$$t_i = \begin{cases} \sum_{i=1}^{k} \dfrac{l_i}{v_{45} \cdot (\tan(c_i))^b} & c_i > c_0 \\ \sum_{i=1}^{k} \dfrac{l_i}{v_{45} \cdot (\tan(c_0))^b} & c_i \le c_0 \end{cases} \tag{7}$$

where $b$ is a parameter that reflects how sensitive the wave velocity is to slope. The value of the parameter $b$ is related to the condition of the underlying surface of the catchment.

Compared with Equation (4), Equation (6) is more general and more physically realistic. Because different basins have different underlying conditions, it cannot be known how sensitive the wave velocity is to slope. In this case, $b$ varies in different basins. Equation (6) reflects the relationship between wave velocity and slope more flexibly and can more easily reflect the characteristics of different basins. Thus, Equation (5) is substituted with Equation (7) in the improved NRF routing method.

There are two parameters in the improved NRF routing method (referred to as 'after' in the following) and one parameter in the original NRF routing method (referred to as 'before' in the following). Table 3 shows the routing parameter value sets for calibration. They were chosen based on computer capability limitations and the physical meaning of each parameter. There are 7 routing parameter value sets before and 42 sets after, composed of six kinds of parameter $b$ and seven kinds of parameter $v_{45}$.

## Evaluation criteria

The model before and after the routing method improvement was calibrated and validated in all catchments. The warm-up period was 1 year for all catchments.

The Nash–Sutcliffe (NSE) efficiency (Nash & Sutcliffe 1970) was used as the criterion for evaluating overall runoff simulation performance in this study.

$$\text{NSE} = 1 - \frac{\sum_{i=1}^{n} (O_i - S_i)^2}{\sum_{i=1}^{n} (O_i - \overline{O_i})^2} \tag{8}$$

where $O_i$ is the observed runoff, $S_i$ is the simulated runoff, and $n$ is the length of the time step.

**Table 3** | The parameters of the routing methods and their prior range for calibration

|        | Parameter | Explanation | Values |
|--------|-----------|-------------|--------|
| Before | $v_{45}$ (m/s) | The wave velocity of a grid whose slope is 45° | 4, 5, 6, 7, 8, 9, 10 |
| After  | $b$ (–) | Power exponent reflecting how sensitive is the $v$ to slope | 0.2, 0.25, 0.3, 0.35, 0.4, 0.45 |
|        | $v_{45}$ (m/s) | The wave velocity of a grid whose slope is 45° | 4, 5, 6, 7, 8, 9, 10 |
|        | The combination of all values yields 42 parameter sets | | |

To measure the peak flow simulation performance, the time lag and relative error of peak flow were also calculated.

$$Q_{\text{re}} = \frac{Q_{\text{sim max}} - Q_{\text{obs max}}}{Q_{\text{obs max}}} \tag{9}$$

$$\Delta T = T_{\text{sim}} - T_{\text{obs}} \tag{10}$$

where $Q_{\text{re}}$ is the relative error of the peak flow, $Q_{\text{sim max}}$ is the simulated maximum peak flow, $Q_{\text{obs max}}$ is the observed maximum peak flow, $T_{\text{sim}}$ is the day when $Q_{\text{sim max}}$ appears, and $T_{\text{obs}}$ is the day when $Q_{\text{obs max}}$ appears. $\Delta T$ is the time lag of the simulated peak flow relative to the observed peak flow.

$Q_{\text{re}}$ and $\Delta T$ of all selected flood events in a catchment were averaged to reflect the overall simulation performance of the peak flow in that catchment as follows:

$$\overline{Q_{\text{re}}} = \frac{1}{l} \sum_{j=1}^{l} |Q_{\text{re},j}| \tag{11}$$

$$\overline{\Delta T} = \frac{1}{l} \sum_{j=1}^{l} |\Delta T_j| \tag{12}$$

where $\overline{\Delta T}$ is the averaged time lag of the peak flow in the catchment, $\overline{Q_{\text{re}}}$ is the averaged relative error of the peak flow in the catchment, and $l$ is the number of flood events in the catchment.

The parameters of the routing method were calibrated using the Monte Carlo algorithm (Barraquand & Latombe 1990), and the parameters of the runoff-generation model were calibrated using Covariance Matrix Adaption Evolution (CMAES) (Hansen & Ros 2010). The Monte Carlo algorithm was used to search for the best routing parameter set. First, 300 runoff-generation parameter value sets were produced using LATIN-Hypercube sampling (Mckay *et al.* 2000) according to the prior range of the parameters. Table 3 shows the routing parameter sets. Second, for each routing parameter set, all of the runoff-generation parameter value sets were used to drive the hydrological model, and then the NSE was calculated based on the simulated runoff and the observed runoff. Third, the best routing parameters were selected based on the NSE. Then, the Covariance Matrix Adaption Evolution algorithm was used

to search for the best runoff-generation parameters under the condition that the routing parameters are fixed.

## RESULTS AND DISCUSSION

### Modeling performance assessment with the improved NRF

Both routing methods were taken as the routing module of the WASMOD. To all catchments, the model was calibrated by using 7 years' data series and validated by using another 4 years' data series during the period of 1964–2008. Figure 2 shows the performance of the daily runoff simulation before and after the improvement.

Figure 2 shows that the model with the improved NRF routing method performs better than the model with the original NRF routing method for all of the study catchments to varying extents. Taking the Baihe catchment and the Waizhou catchment as examples, the Baihe catchment has an NSE of 0.87 in the calibration period and 0.74 in the validation period after the improvement, while the NSE is 0.43 in the calibration period and 0.31 in the validation period before the improvement. The Waizhou catchment has an NSE of 0.82 in the calibration period and 0.78 in the validation period after the improvement, while the NSE is 0.58 in the calibration period and 0.59 in the validation period before the improvement. The mean improvement in the NSE in both the calibration period and the validation

period of the 15 catchments is 0.11, with a maximum of 0.44 in the calibration period and 0.43 in the validation period. From Figure 2, it can also be found that the improvement in NSE varies greatly in the 15 catchments of the Yangtze River basin after the improvement of the routing method.

In order to demonstrate the difference in the simulated and observed discharge hydrographs of the original and improved routing methods, daily hydrographs of a representative year 1968 for the Shimen catchment are plotted in Figure 3. It shows that with the original NRF routing method, the simulated flood peak is often later than the observed flood peak. The improved NRF can better simulate the flood peak. Tables 4 and 5 show the optimal parameters of the hydrological model with the original and the improved routing method.

In order to assess the flood simulation performance of the model with the improved NRF routing method, the averaged relative errors $\overline{Q_{re}}$ and averaged time lags $\overline{\Delta T}$ of all flood events in each catchment were calculated using Equations (11) and (12) and are shown in Figure 4. The flood events whose peak flow was greater than three times the average runoff of catchment were selected in this study. It can be seen that the model with the improved NRF routing method provides better flood simulation performance than the model with the original NRF routing method. After the improvement, the averaged time lags of the peak flow in almost all catchments are less than one day, except for the Shigu and Waizhou catchments (Figure 4,
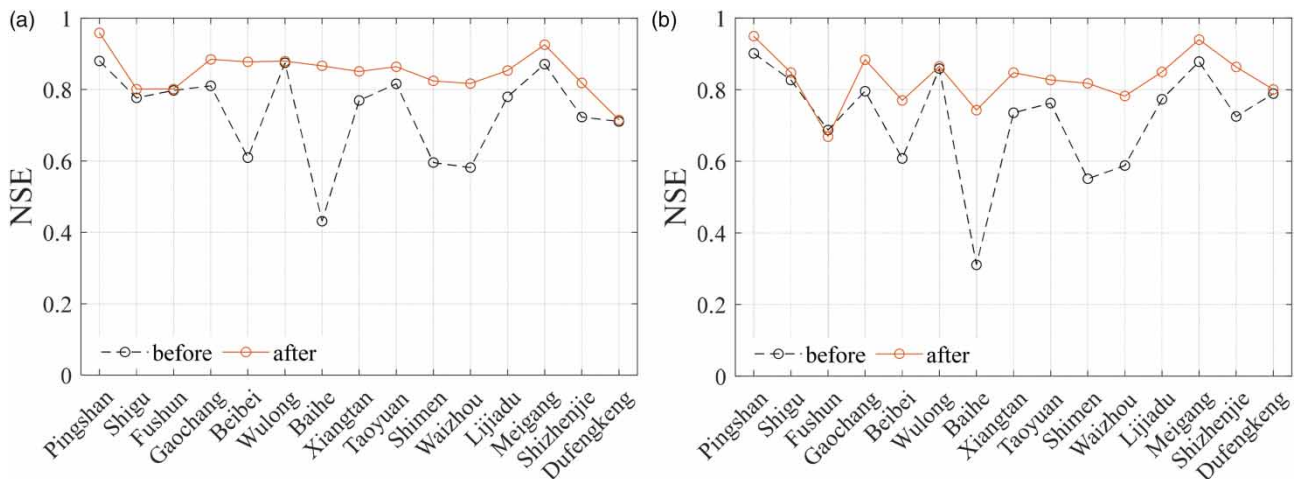


**Figure 2** | NSE in (a) the calibration period and (b) the validation period in all catchments by the NRF routing method before and after the improvement.
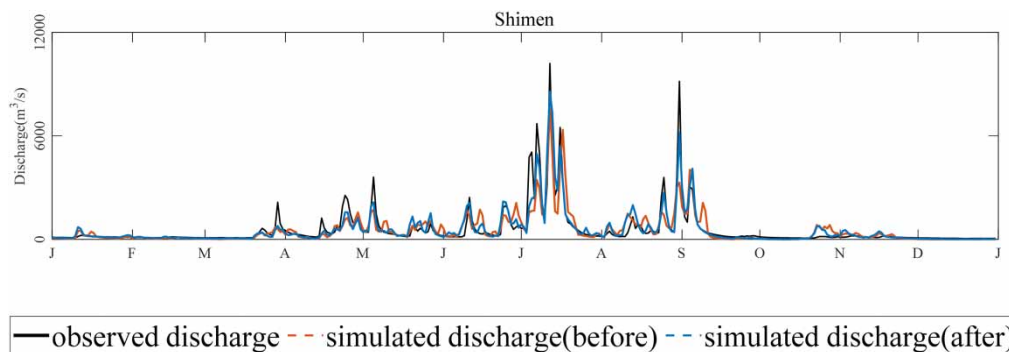
Figure 3 | The simulated and observed discharge hydrographs for the Shimen catchment in 1968 by the NRF routing method before and after the improvement.

Table 4 | The optimal parameter values of the hydrological model with the original routing method

| Catchment | $v_{45}$ | $b$ | $a_1$ | $a_2$ | $a_4$ | $c_1$ | $c_2$ | $c_4$ | $c_5$ |
|---|---|---|---|---|---|---|---|---|---|
| Pingshan | 0.5 | 6 | 6.00 | 0.00 | 0.65 | 0.0075 | 0.00005 | 0.10 | 0.58 |
| Shigu | 0.5 | 10 | 6.00 | 0.00 | 0.99 | 0.0124 | 0.00008 | 0.27 | 0.50 |
| Fushun | 0.5 | 10 | 6.00 | −1.83 | 0.93 | 0.0092 | 0.00055 | 0.35 | 0.78 |
| Gaochang | 0.5 | 10 | 5.78 | −1.51 | 1.00 | 0.0064 | 0.00018 | 0.10 | 0.64 |
| Beibei | 0.5 | 10 | 0.05 | −5.00 | 0.81 | 0.0145 | 0.00017 | 0.12 | 0.59 |
| Wulong | 0.5 | 9 | – | – | 0.88 | 0.0087 | 0.00022 | 0.41 | 0.91 |
| Baihe | 0.5 | 10 | – | – | 0.71 | 0.1000 | 0.00008 | 0.15 | 0.69 |
| Xiangtan | 0.5 | 10 | – | – | 0.95 | 0.0015 | 0.00002 | 0.66 | 1.11 |
| Taoyuan | 0.5 | 10 | – | – | 0.94 | 0.0040 | 0.00007 | 1.00 | 1.14 |
| Shimen | 0.5 | 9 | – | – | 0.88 | 0.0879 | 0.00575 | 1.00 | 0.97 |
| Waizhou | 0.5 | 10 | – | – | 0.96 | 0.0088 | 0.00003 | 0.26 | 0.71 |
| Lijiadu | 0.5 | 10 | – | – | 0.96 | 0.0017 | 0.00001 | 1.00 | 1.10 |
| Meigang | 0.5 | 10 | – | – | 0.96 | 0.0026 | 0.00001 | 1.00 | 1.20 |
| Shizhenjie | 0.5 | 10 | – | – | 0.93 | 0.0010 | 0.00001 | 1.00 | 1.36 |
| Dufengkeng | 0.5 | 10 | – | – | 0.94 | 0.0089 | 0.00046 | 1.00 | 0.90 |

left panel). The averaged relative error of the peak flow in all catchments decreases in nearly all of the catchments (Figure 4, right panel). The amelioration is most evident in the Waizhou catchment, where $\overline{Q_{re}}$ equals 0.32 with the original routing method and 0.17 with the improved routing method. The relative error of the peak flow decreases to the minimum error range of −0.1 to 0.1 after the improvement in the routing method in all of the catchments except for the Dufengkeng and Fushun catchments.

To evaluate the ability of simulating the occurrence of flood peaks, the time lags $\Delta T$ in all selected flood events in each catchment were analyzed. Figure 5 plots the frequency distributions histogram of time lags $\Delta T$ in each catchment with the original and improved NRF routing method. Frequency is the number of flood events that $\Delta T$ in a certain value is divided by the total number of flood events in this catchment. When the time lag $\Delta T$ is positive, it means that the simulated flood peak is later than the actual one. On the contrary, when the time lag $\Delta T$ is negative, it means that the simulated flood peak is earlier than the actual one. When $\Delta T$ equals zero, the hydrological model simulates the time of flood peak accurately. Figure 5 shows that with the original routing method, the frequency of positive time lag $\Delta T$ is larger than the frequency of negative time lag $\Delta T$.

**Table 5** │ The optimal parameter values of the hydrological model with the improved routing method

| Catchment | $v_{45}$ | $b$ | $a_1$ | $a_2$ | $a_4$ | $c_1$ | $c_2$ | $c_4$ | $c_5$ |
|---|---|---|---|---|---|---|---|---|---|
| Pingshan | 0.2 | 5 | 6.00 | 0.00 | 0.47 | 0.0038 | 0.00015 | 0.11 | 0.58 |
| Shigu | 0.45 | 8 | 6.00 | 0.00 | 0.99 | 0.0125 | 0.00012 | 0.26 | 0.50 |
| Fushun | 0.45 | 10 | 0.99 | −2.32 | 0.12 | 0.0148 | 0.00224 | 0.14 | 0.66 |
| Gaochang | 0.2 | 5 | 2.88 | −6.00 | 1.00 | 0.0059 | 0.00028 | 0.91 | 0.64 |
| Beibei | 0.3 | 7 | 5.45 | −1.81 | 0.50 | 0.0120 | 0.00054 | 0.27 | 0.74 |
| Wulong | 0.45 | 8 | – | – | 0.88 | 0.0082 | 0.00026 | 0.40 | 0.90 |
| Baihe | 0.3 | 10 | – | – | 0.81 | 0.0090 | 0.00051 | 1.00 | 1.14 |
| Xiangtan | 0.25 | 4 | – | – | 0.22 | 0.0039 | 0.00012 | 0.21 | 0.79 |
| Taoyuan | 0.2 | 4 | – | – | 0.94 | 0.0040 | 0.00019 | 1.00 | 1.09 |
| Shimen | 0.25 | 8 | – | – | 0.91 | 0.0123 | 0.00080 | 1.00 | 1.19 |
| Waizhou | 0.35 | 8 | – | – | 0.97 | 0.0038 | 0.00007 | 0.91 | 0.89 |
| Lijiadu | 0.4 | 9 | – | – | 0.94 | 0.0044 | 0.00015 | 1.00 | 0.91 |
| Meigang | 0.4 | 9 | – | – | 0.94 | 0.0081 | 0.00043 | 1.00 | 0.96 |
| Shizhenjie | 0.25 | 4 | – | – | 0.95 | 0.0078 | 0.00085 | 1.00 | 0.89 |
| Dufengkeng | 0.45 | 9 | – | – | 0.76 | 0.0124 | 0.00104 | 0.24 | 0.78 |
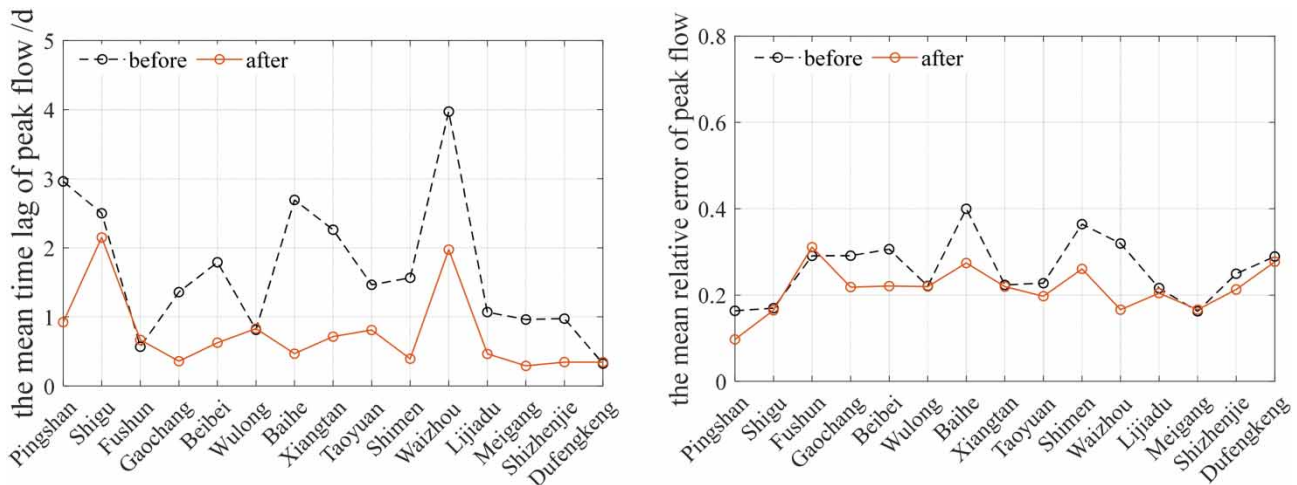


**Figure 4** │ The averaged time lag of peak flow (left panel) and relative error of peak flow (right panel) in all catchments by the NRF routing method before and after the improvement.

That indicates that the simulated peak flow is often delayed compared with the observed peak flow with the original NRF routing method. There is a higher frequency of zero time lag of peak flow ($\Delta T$ equals zero) in most of the catchments with the improved routing method than that with the original routing method. Particularly, in the Gaochang, Shizhengjie, and Meigang catchments, the frequency of zero time lag of peak flow is greater than 0.8 in the model with the improved routing method and less than 0.4 in the

model with the original routing method. Those phenomena indicate that the improved routing methods can better serve the flood simulation.

These results indicate that the model with the improved routing method performs better in both peak flow simulation and long-term runoff simulation than the model with the original routing method. Besides this, NRF's advantage of being able to preserve the travel time information in the PRF is maintained in the improved model.
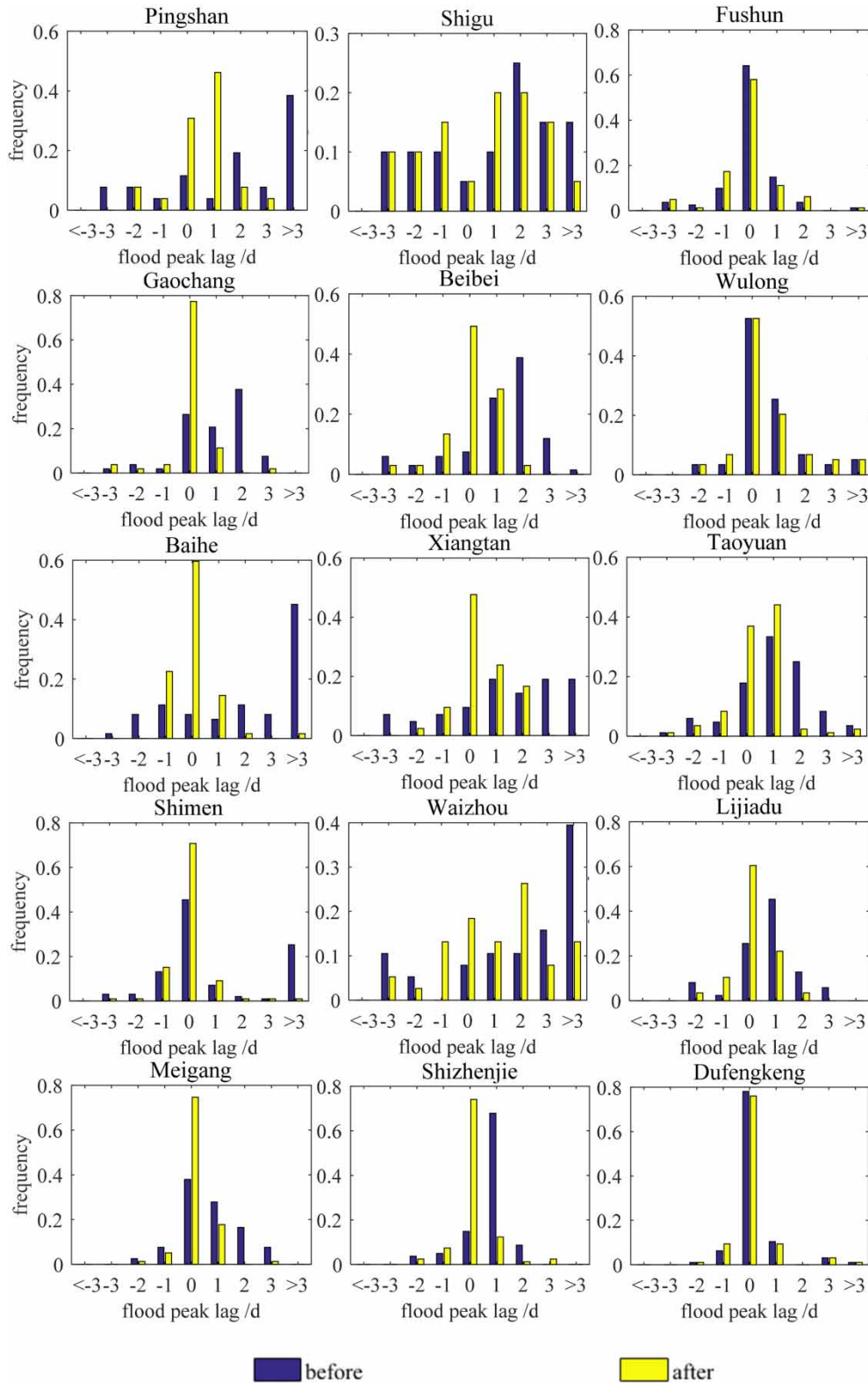
**Figure 5** | The frequency distributions of time lags (day) for all of the catchments by the NRF routing method before and after the improvement.

## Analysis of the routing time calculated by the improved NRF

Figure 6(a) and 6(b) show the distributions of the travel time of all grids in all catchments that were calculated by the original and the improved routing methods. Figure 6(d) plots the mean grid travel time and mean slope of all of the catchments. The simulated travel time was evaluated based on two hydrological stations in each catchment: the outlet station and the specific upstream hydrological station that made the distance between the two hydrological stations as large as possible. Figure 6(c) plots the runoff travel times between the upstream hydrological station and the outlet station that were calculated

by the original routing method and the improved routing method. The runoff travel times were compared with the travel time provided by Zhang *et al.* (2006) as a benchmark.

For most catchments, the travel time between grids that was calculated by the improved routing method was shorter than that calculated by the original routing method (Figure 6(a) and 6(b)). Besides this, the travel time between the specific upstream hydrological station and the outlet station was shorter and closer to the benchmark value for all the catchments (Figure 6(c)). The main reason why the travel time that was calculated by the improved routing method was longer than the benchmark value in some catchments is that the routing parameters $v_{45}$ and $b$ are
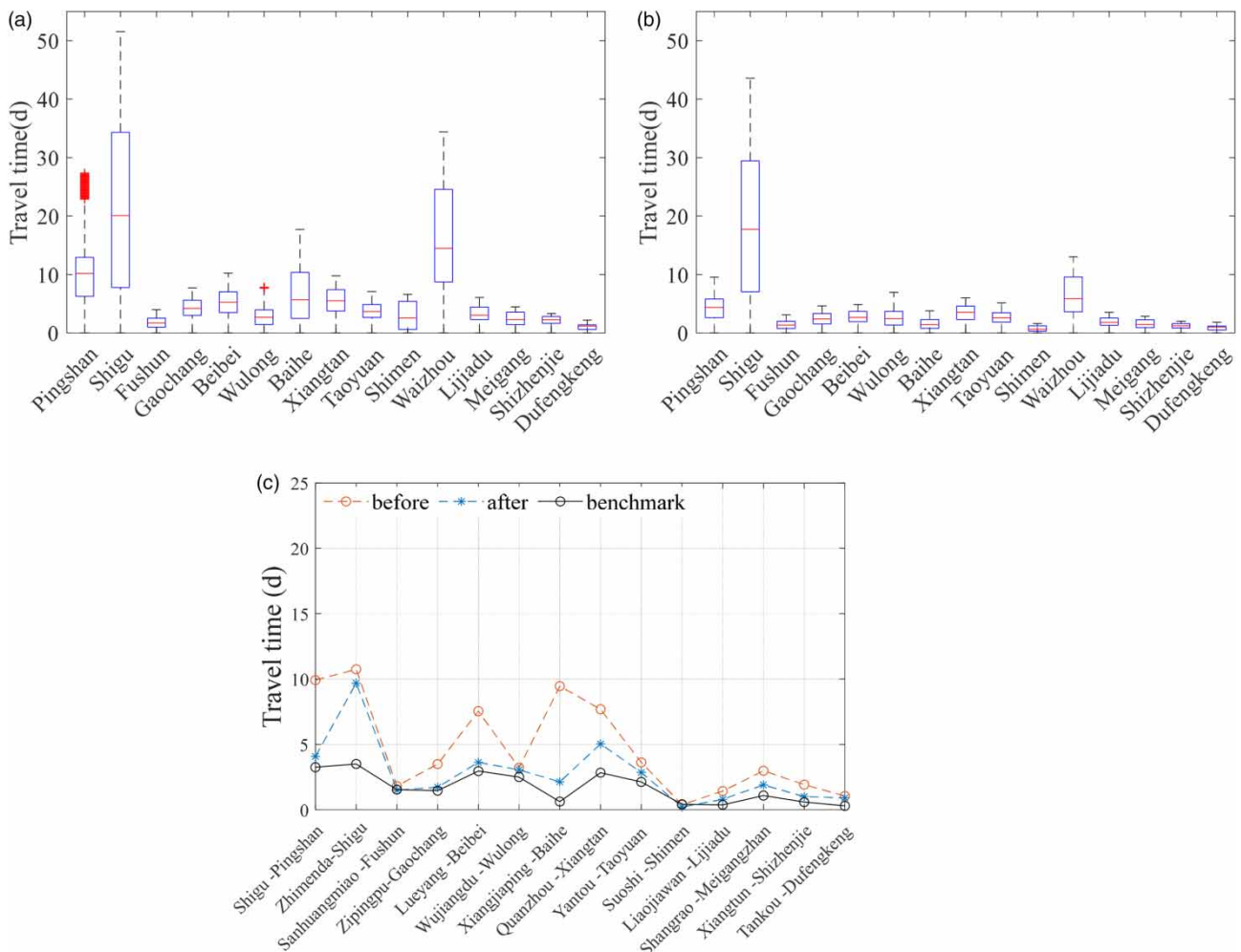


**Figure 6** │ The evaluation of the travel times. (a) Box plots of the travel time in all catchments calculated by the model with the NRF routing method before the improvement and (b) after the improvement; (c) the averaged travel time in all of the catchments simulated by the model before and after the improvement compared with observations.

spatially constant over the whole catchment. However, routing refers to the process in which rainfall in a catchment evolves along a certain path into discharge at the outlet. The rainfall is first routed by a hillslope and then routed by the river before being transferred into discharge. Hillslope routing and river routing are two forms of routing (Kirkby & Beven 1993). Usually, the runoff travels faster in river routing than in hillslope routing. However, the hillslope travel time and the river travel time are not separated in both the original and improved NRF routing methods. The parameters $v_{45}$ and $b$ reflect the state of the whole basin; however, the benchmark value reflects the travel time that is needed in the selected river section. Thus, the travel time in the river that is calculated by the improved routing method will be a little longer than the benchmark value. However, the travel time that was calculated in the Shigu catchment is much longer than the benchmark value, which is due to the Shigu catchment's underlying surface. The shape factor of the Shigu catchment is the largest of all of the studied catchments, which means that the shape of the Shigu catchment is narrow and long and the water system's development is immature. The above factors lead to much more hillslope routing and a longer travel time in the Shigu catchment. In addition, the snowmelt and groundwater are the main sources of runoff in the Shigu catchment. The snowmelt runoff moves more slowly down the hillslope than the rainfall runoff, so the optimal routing parameters that were calibrated using the observed runoff lead to a longer travel time in the Shigu catchment compared with the benchmark value, which only considers routing in the river.

The travel time that was calculated using the original routing method produces a late peak flow and a smaller amount of flow (Figure 4). An unreasonable travel time is one of the main causes of a hydrological model's poor performance in long-term runoff simulation. The improved routing method provides a more realistic travel time between the grids compared with the benchmark value.

When analyzed in conjunction with Figures 2 and 6, it can be found that the NSE and the travel time in all catchments have a close relationship. From Figure 2, it can be seen that the NSE that was calculated by the original NRF is lower in some catchments, i.e., the Waizhou, Shimen, Beibei, and Baihe catchments. As shown in Figure 6(c),

the runoff travel times in these catchments, as calculated using the original routing method, were unrealistic and at least twice as long as the runoff travel times that were calculated using the improved routing model. On the other hand, for the Dufengkeng, Fushun, and Wulong catchments, we found no obvious change in the travel times that were calculated using the original and improved routing methods. The original and improved routing methods also provided a similar NSE in these catchments.

## Analysis of the wave velocity calculated by the improved NRF

Figure 7 shows the theoretical curves of wave velocity versus slope. Figure 8(a) and 8(c) plot the calibrated curves that
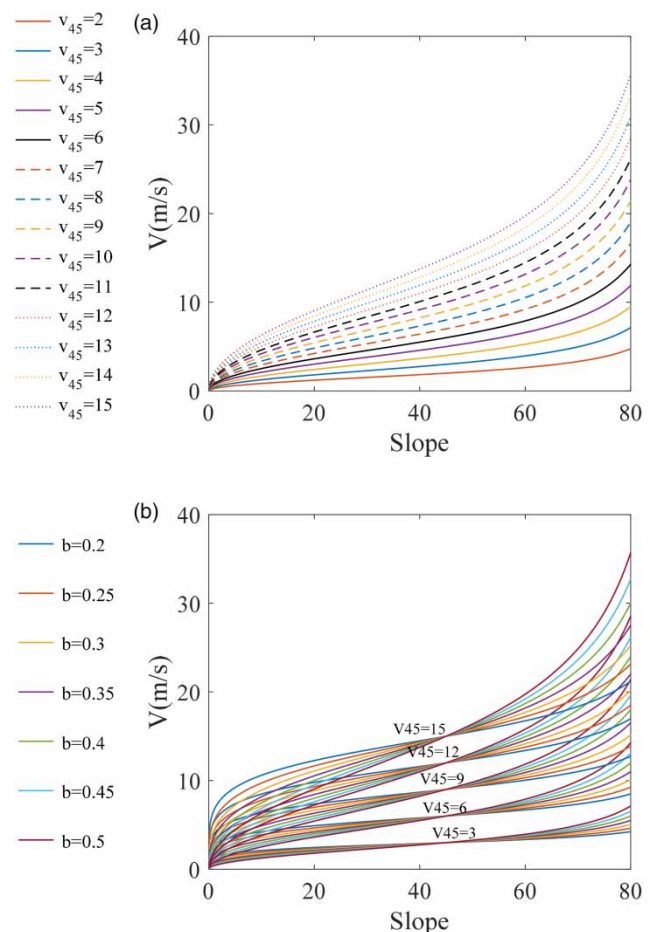


**Figure 7** | The theoretical curve of velocity and slope: (a) wave velocity changes with slope with the parameter $v_{45}$ before the improvement and (b) wave velocity changes with slope with the two parameters $v_{45}$ and $b$ after the improvement.

were calculated by the original routing method and the improved routing method (Table 3), respectively. From the analysis in the section Analysis of the routing time calculated by the improved NRF, it is known that the improved routing method is able to achieve a more reasonable travel time. The reason for this is that the improved routing method has a more flexible wave velocity–slope curve (Figure 7) that can better reflect the real world.

It can be seen from Figure 7(b) that the wave velocity of a grid is determined by the parameters $b$ and $v_{45}$ together. If the parameter $b$ remains constant, the wave velocity increases as $v_{45}$ increases. If the parameter $v_{45}$ remains constant, the wave velocity increases as $b$ decreases at grids with a slope of less than 45°; however, the wave velocity increases as $b$ increases at grids with a slope of greater than 45°. The effect that slope has on the wave velocity varies across catchments due to the differences in the hydrology of the underlying surface, which can be adjusted by the parameter $b$. The bigger $b$ is, the more sensitive the wave velocity is to slope. When $b$ is equal to zero, the slope has no effect on wave velocity, which will be a constant. A larger wave velocity results in a shorter runoff travel time in a catchment.

Each routing parameter value set refers to a certain curve between slope and calibrated wave velocity. The original NRF only produces three kinds of curves for the 15 catchments (Figure 8(a)). The curves of 13 catchments coincide because they have the same optimal value of $v_{45}$. However, the improved NRF produces a different calibrated curve for each catchment (Figure 8(c)). Tables 6 and 7 present the optimal values of $v_{45}$ that were calibrated by the original routing method with a strict range of 4–10 m/s (cali1), as in Table 3, and with a wider prior range of 4–31 m/s (cali2), respectively. Due to computer capability limitations, the increment of parameter $v_{45}$ above 10 m/s is 3 m/s. Figure 8(e) plots the calibrated curves between slope and calibrated wave velocity in cali2. In combination with the optimal value of $v_{45}$ shown in Tables 6 and 7, it can be seen that the optimal value of $v_{45}$ in cali1 is the same as 10 m/s, reaching the upper limit of the prior range for nearly all of the catchments. When the prior range for calibration is fixed to be 4–10 m/s, the larger the value of $v_{45}$, the shorter the travel time, which is closer to the reality in most catchments. This results in a

larger NSE value. Thus, the calibrated value of $v_{45}$ reaches the upper limit of the prior range for calibration in 13 catchments, resulting in only three kinds of curves between slope and calibrated wave velocity in 15 catchments. Moreover, in many basins, the optimal value of $v_{45}$ in cali2 is larger than 10 m/s and has a maximum of 31 m/s; thus, the grid wave velocity is too large to be realistic (Figure 8(e)). Figure 8(b), 8(d) and 8(f) show the distributions of the wave velocity of all grids in all catchments before the improvement with the strict prior range of parameter $v_{45}$ for calibration; after the improvement with the strict prior range of parameter $v_{45}$ for calibration; before the improvement with the wider prior range of parameter $v_{45}$ for calibration. It also shows that the grid wave velocity is too large to be realistic before the improvement with the wider prior range of parameter $v_{45}$ for calibration. The model can provide good runoff simulation performance because the excessively large value of $v_{45}$ compensates for the problem of the routing time being too long due to the unreasonable distribution of the grids' wave velocity. This indicates that the original routing method cannot adapt to the variation in the underlying surface of the different basins. This is consistent with the results from Gong *et al.* (2011), who found that the optimal value of $v_{45}$ was physically unrealistic as it was determined to be greater than 26 m/s with the original Hydro1 k-driven NRF routing method.

The original NRF routing method uses a constant (0.5) to reflect the influence that the slope has on the wave velocity; however, it fails to adapt to the variation in the underlying surface of the different basins. The improved routing method makes it possible to fit the actual physical relationship between the slope and wave velocity in a more flexible way. The reasonable distribution of wave velocity leads directly to a more accurate simulation of the travel time, which in turn leads to a better simulation of the runoff.

The improved NRF routing method belongs to hydrological methods rather than hydraulics methods. There are some other hydrological routing methods calculating the travel time of each grid and then routing the runoff to discharge. But the parameter to calibrate and influence factors that have been taken into consideration are different in different methods.
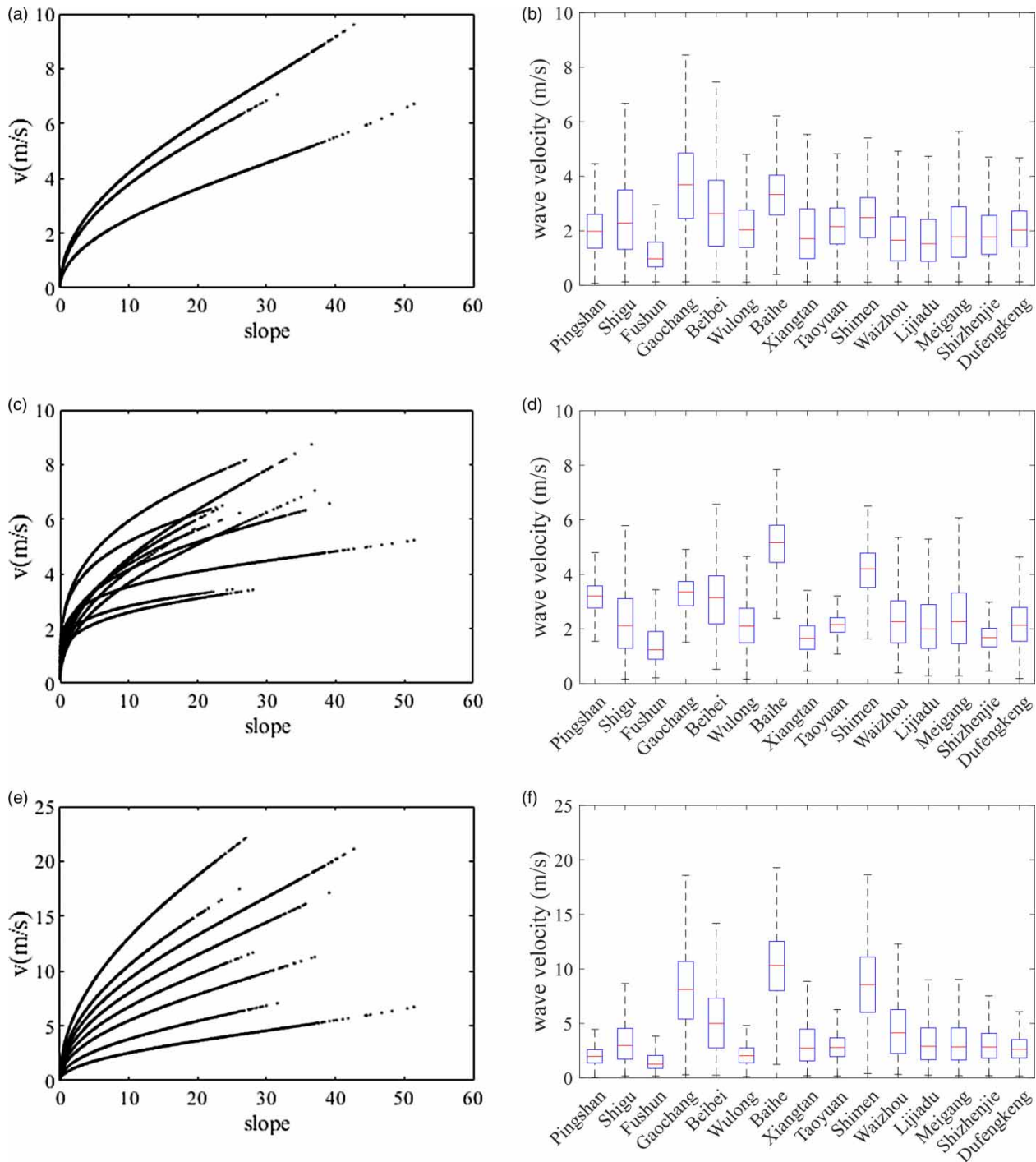
**Figure 8** | Curves and box plots of calibrated wave velocity versus slope (a) and (b) before the improvement with the strict prior range of parameter $v_{45}$ for calibration, (c) and (d) after the improvement with the strict prior range of parameter $v_{45}$ for calibration, and (e) and (f) before the improvement with the wider prior range of parameter $v_{45}$ for calibration.

For the routing method in Ducharne *et al.* (2003), only the slope between two grids will influence the velocity. For the routing method in Guo *et al.* (2004), not only the slope, but also the hydraulic radius, the roughness of the cell and the scale factor about the cell size will influence the wave velocity. For the routing method in Bunster *et al.* (2019), it proposed a

**Table 6** │ The values of the optimal routing parameter $v_{45}$ with the prior range of 4–10 m/s

| Catchment | Pingshan | Shigu | Fushun | Gaochang | Beibei |
|---|---|---|---|---|---|
| Optimal value (m/s) | 6 | 10 | 10 | 10 | 10 |
| NSE | 0.88 | 0.78 | 0.80 | 0.81 | 0.61 |
| Catchment | Wulong | Baihe | Xiangtan | Taoyuan | Shimen |
| Optimal value (m/s) | 9 | 10 | 10 | 10 | 9 |
| NSE | 0.88 | 0.43 | 0.77 | 0.82 | 0.60 |
| Catchment | Waizhou | Lijiadu | Meigang | Shizhenjie | Dufengkeng |
| Optimal value (m/s) | 10 | 10 | 10 | 10 | 10 |
| NSE | 0.88 | 0.43 | 0.77 | 0.82 | 0.60 |

**Table 7** │ The values of the optimal routing parameter $v_{45}$ with a wider prior range of 4–31 m/s

| Catchment | Pingshan | Shigu | Fushun | Gaochang | Beibei |
|---|---|---|---|---|---|
| Optimal value | 6 | 13 | 13 | 22 | 19 |
| NSE | 0.88 | 0.82 | 0.80 | 0.89 | 0.87 |
| Catchment | Wulong | Baihe | Xiangtan | Taoyuan | Shimen |
| Optimal value | 9 | 31 | 16 | 13 | 31 |
| NSE | 0.88 | 0.83 | 0.85 | 0.85 | 0.79 |
| Catchment | Waizhou | Lijiadu | Meigang | Shizhenjie | Dufengkeng |
| Optimal value | 25 | 19 | 16 | 16 | 13 |
| NSE | 0.80 | 0.85 | 0.93 | 0.81 | 0.72 |

travel time formulation that accounts for the dynamics of the upstream contributions, compared to the previous methods. In that method, the dynamics of the upstream contributions and slope will influence the wave velocity. Du *et al.* (2009) proposed a time variant routing method, the spatially distributed direct hydrograph travel time method (SDDH), in which time variant runoff, grid length, the roughness of the cell, and slope are used to calculate the wave velocity.

Some data such as hydraulic radius may not be available when applying the large-scale hydrological model. Thus, the routing method requiring too much input information may not preferable in a large-scale hydrological model. In the improved NRF routing method, all the necessary information can be taken from the DEM. Compared with the routing methods that only take the slope into consideration, the improved NRF can be adapted to more basins. Overall, the improved NRF routing method is simple and effective for a large-scale hydrological model.

## Factors that influence the wave velocity calculation

The wave velocity of a grid is affected not only by the grid's slope but also by many other factors, including the basin shape factor, rainfall intensity, vegetation cover, branching ratio, basin area, climate, and form of drainage. The factors that influence the travel time are so numerous that they may compensate for each other to some extent. It is difficult to calculate the wave velocity of each grid precisely. So, these influencing factors were generalized to be reflected by the parameter $v_{45}$, the parameter $b$, and slope in this study. The parameter $b$ varies across basins due to differences in basin characteristics, and it represents the underlying surface.

The underlying surface influences the wave velocity and travel time in many ways. There is no strict and deterministic functional relationship between basin characteristic and mean wave velocity in a large-scale hydrological model.

Multivariate regression analysis (Alexopoulos 2010; Zhang et al. 2014) is a mathematical analysis method that uses the least squares method to model the relationship between a dependent variable and multiple independent variables. In this study, we used it to examine the relationship between the mean wave velocity of grids $\bar{v}$ (m/s) calculated with the improved routing method and several influencing factors. The result equation will not be used to calculate the wave velocity directly. But this method can identify basin characteristics that have a greater impact on the mean wave velocity. Some variables that are related to wave velocity are chosen (Table 1): mean discharge at the outlet station $\overline{Q}$ (m³/s); area $A$ (km²); shape factor $F$; mean slope $S$ (°); river length $L_r$ (m); and range of elevation $\Delta H$ (m). The area, shape factor, and river length are basin geometric factors which affect the path and sequence of runoff and then influence the mean wave velocity. The slope and range of elevation influence the wave velocity, because potential energy will be converted into kinetic energy. In the process of runoff routes, runoff will continually merge and diverge, and the speed between water will affect each other. Thus, the mean discharge at the outlet station is also taken as an independent variable.

Based on data of the 15 studied catchments, multiple linear regression analysis was done using the above factors as independent variables and mean wave velocity as the dependent variable. The value of $R^2$ was found to be equal to 0.73 and the significance level of the $F$-test was 0.051, which indicates that the mean wave velocity is associated (at the 90% level) with the above factors. The final regression equation is shown as Equation (13). The standardized regression coefficients of those variables are $-0.23$ ($\overline{Q}$), $-1.37$ ($A$), 0.44 ($F$), 1.42 ($S$), $-0.55$ ($L_r$), and 0.79 ($\Delta H$). It can be inferred that the slope has the greatest positive effect on wave velocity and the area has the most negative effect.

$$\bar{v} = -0.0001884\overline{Q} - 0.00001691A + 0.8231F \\ + 0.6517S - 0.0003146\Delta H + 0.0004925L_r \qquad (13)$$

where $\bar{v}$ (m/s) is the mean wave velocity of the grids; $\overline{Q}$ (m³/s) is the mean discharge at the outlet station; $A$ (km²) is the area; $F$ is the shape factor; $S$ (°) is the mean slope; $L_r$ (m) is the river's length; and $\Delta H$ (m) is the range of elevation.

There are other factors that are not included in Equation (13), and for $R^2$ it is not equal to 1. However, we have yet to find more accurate and detailed rules. The mean wave velocity that was predicted by Equation (13) was compared with the mean wave velocity that was calculated with the improved routing method as shown in Figure 9, which shows an overall good result.

In the future study, more data on the factors that influence wave velocity, such as soil, vegetation cover, and the branching ratio, should be inputted into the method in order to examine the relationship between routing parameters and basin characteristics. If appropriate, the improved routing model has the potential to be applied to data-sparse areas by a parameter transformation based on the distribution in a subzone of climate, soil, and vegetation, or even to calculate the travel time without parameters, which would enable this model to be used to simulate the hydrological effect of climate and land-use change.

## CONCLUSIONS

In this paper, a flow routing algorithm was developed by combining an aggregation NRF with a velocity function.
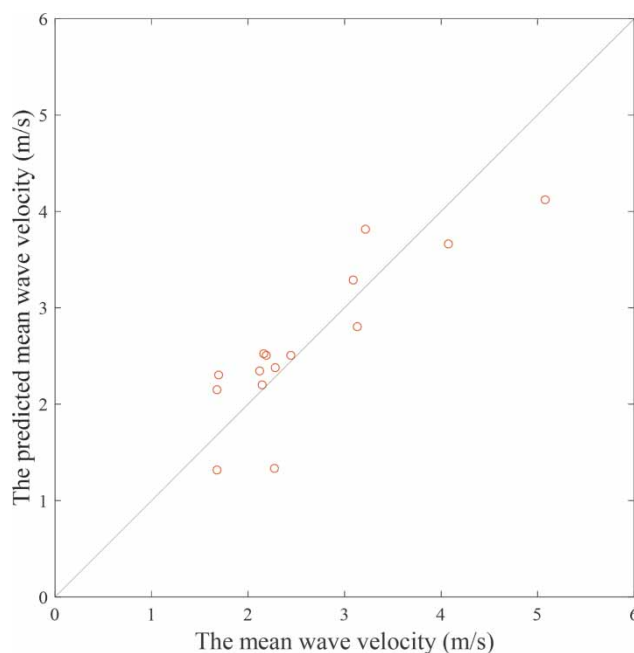


**Figure 9** | A comparison between the predicted and calculated mean wave velocity of grids.

The improved routing NRF method uses a parameter $b$ that can reflect how sensitive the wave velocity is to a slope. The routing methods before and after the improvement were applied to 15 catchments in the Yangtze River using a daily WASMOD-M model based on Hydro1 k. The main conclusions can be summarized as follows:

(1) The original NRF routing method was found to provide unsatisfactory runoff simulation performance in most of the studied catchments, with an unreasonable calibrated travel time and wave velocity of the grids, for it cannot adapt to the different underlying conditions in the different catchments.

(2) After the improvement in the NRF routing method, the relationship between wave velocity and slope was found to be more flexible. It can simulate the complexity of the wave velocity distribution more effectively in all types of basins, resulting in a reasonable runoff travel time.

(3) The runoff travel time that was calculated by the model with the improved NRF routing method was found to be shorter and more reasonable, which leads to better runoff simulation performance.

(4) The model with the improved NRF routing method was found to yield better results with respect to long-term daily runoff time series and peak flow amounts than the model with the original NRF routing method. The improved model was found to perform better in catchments with different characteristics. The improved model also retains the best advantage of NRF; i.e., it records all of the travel time information from the PRF.

## ACKNOWLEDGEMENT

## REFERENCES

Abou Rafee, S. A., Uvo, C. B., Martins, J. A., Domingues, L. M., Rudke, A. P., Fujita, T. & Freitas, E. D. 2019 Large-scale hydrological modelling of the Upper Paraná River Basin. *Water* **11** (5), 882. doi:10.3390/w11050882.

Alexopoulos, E. C. 2010 Introduction to multivariate regression analysis. *Hippokratia* **14** (Suppl. 1), 23. doi:10.1111/j.1365-2362.2009.02222.x.

Arora, V. K. & Boer, G. J. 1999 A variable velocity flow routing algorithm for GCMs. *Journal of Geophysical Research: Atmospheres* **104** (D24), 30965–30979. doi:10.1029/1999jd900905.

Arora, V., Seglenieks, F., Kouwen, N. & Soulis, E. 2001 Scaling aspects of river flow routing. *Hydrological Processes* **15** (3), 461–477. doi:10.1002/hyp.161.

Barraquand, J. & Latombe, J. C. 1990 A Monte-Carlo algorithm for path planning with many degrees of freedom. *IEEE International Conference on Robotics and Automation*. doi:10.1109/ROBOT.1990.126256.

Beven, K. 2001 How far can we go in distributed hydrological modelling? *Hydrology and Earth System Sciences* **5** (1), 1–12. doi:10.5194/hess-5-1-2001.

Beven, K. J. & Kirkby, M. J. 1979 A physically based, variable contributing area model of basin hydrology/Un modèle à base physique de zone d'appel variable de l'hydrologie du bassin versant. *Hydrological Sciences Journal* **24** (1), 43–69. doi:10.1080/02626667909491834.

Bunster, T., Gironás, J. & Niemann, J. D. 2019 On the influence of upstream flow contributions on the basin response function for hydrograph prediction. *Water Resources Research* **55** (6), 4915–4935. doi:10.1029/2018WR024510.

Chen, L., Chang, J., Wang, Y. & Zhu, Y. 2019 Assessing runoff sensitivities to precipitation and temperature changes under global climate-change scenarios. *Hydrology Research* **50** (1), 24–42. doi:10.2166/nh.2018.192.

Du, J., Xie, H., Hu, Y., Xu, Y. & Xu, C.-Y. 2009 Development and testing of a new storm runoff routing approach based on time variant spatially distributed travel time method. *Journal of Hydrology* **369** (1–2), 44–54. doi:10.1016/j.jhydrol.2009.02.033.

Ducharne, A., Golaz, C., Leblois, E., Laval, K., Polcher, J., Ledoux, E. & de Marsily, G. 2003 Development of a high resolution runoff routing model, calibration and application to assess runoff from the LMD GCM. *Journal of Hydrology* **280** (1–4), 207–228. doi:10.1016/S0022-1694(03)00230-0.

Fan, M., Mawuko, D. O., Shibata, H. & Ou, W. 2019 Spatial conservation areas for water yield hydrological ecosystem services with their economic values effects under climate change: a case study of Teshio watershed located in northernmost of Japan. *Hydrology Research* **50** (6), 1679–1709. doi:10.2166/nh.2019.009.

Fekete, B. M., Vörösmarty, C. J. & Lammers, R. B. 2001 Scaling gridded river networks for macroscale hydrology:

development, analysis, and control of error. *Water Resources Research* **37** (7), 1955–1967. doi:10.1029/2001wr900024.

Gong, L., Widen-Nilsson, E., Halldin, S. & Xu, C.-Y. 2009 Large-scale runoff routing with an aggregated network-response function. *Journal of Hydrology* **368** (1–4), 237–250. doi:10.1016/j.jhydrol.2009.02.007.

Gong, L., Halldin, S. & Xu, C.-Y. 2011 Global-scale river routing – an efficient time-delay algorithm based on HydroSHEDS high-resolution hydrography. *Hydrological Processes* **25** (7), 1114–1128. doi:10.1002/hyp.7795.

Guo, J., Xu, L. & Leung, L. R. 2004 A new multiscale flow network generation scheme for land surface models. *Geophysical Research Letters* **31** (23), 345–357. doi:10.1029/2004GL021381.

Hansen, N. & Ros, R. 2010 Benchmarking a weighted negative covariance matrix update on the BBOB-2010 noisy testbed. In: *Conference Companion on Genetic and Evolutionary Computation*. doi:10.1145/1830761.1830788.

Huang, P. C. & Lee, K. T. 2017 Efficient DEM-based overland flow routing using integrated recursive algorithms. *Hydrological Processes* **31** (5), 1007–1017. doi:10.1002/hyp.11080.

Kharin, V., Flato, G., Zhang, X., Gillett, N., Zwiers, F. & Anderson, K. 2018. *Earth's Future* **6** (5), 704–715. doi:704-715. 10.1002/2018EF000813.

Kirkby, M. J. & Beven, K. 1993 *Channel Network Hydrology*. John Wiley & Sons, New York.

Kizza, M., Rodhe, A., Xu, C.-Y. & Ntale, H. K. 2011 Modelling catchment inflows into Lake Victoria: uncertainties in rainfall–runoff modelling for the Nzoia River. *Hydrological Sciences Journal* **56** (7), 1210–1226. doi:10.1080/02626667.2011.610323.

Li, L., Xia, J., Xu, C.-Y. & Singh, V. P. 2010 Evaluation of the subjective factors of the GLUE method and comparison with the formal Bayesian method in uncertainty assessment of hydrological models. *Journal of Hydrology* **390** (3), 210–221. doi:10.1016/j.jhydrol.2010.06.044.

Li, Z., Xu, Z. & Li, Z. 2011 Performance of WASMOD and SWAT on hydrological simulation in Yingluoxia watershed in northwest of China. *Hydrological Processes* **25** (13), 2001–2008. doi:10.1002/hyp.7944.

Li, L., Xu, C.-Y. & Jain, S. 2013 Comparison of the global TRMM and WFD precipitation datasets in driving q large-scale hydrological model in Southern Africa. *Hydrology Research* **44** (5), 770–788. doi:10.2166/nh.2012.175.

Li, H., Beldring, S. & Xu, C.-Y. 2014 Implementation and testing of routing algorithms in the distributed Hydrologiska Byråns Vattenbalansavdelning model for mountainous catchments. *Hydrology Research* **45** (3), 322–333. doi:10.2166/nh.2013.009.

Li, L., Shen, M., Hou, Y., Xu, C.-Y., Lutz, A. F., Chen, J., Jain, S. K., Li, J. & Chen, H. 2019 Twenty-first-century glacio-hydrological changes in the Himalayan headwater Beas River basin. *Hydrology Earth System Sciences* **23** (3), 1483–1503. doi:10.5194/hess-23-1483-2019.

Ling, Z., Nan, Z., Xu, L., Yi, X., Hernández, F. & Li, L. 2018 Application of the MacCormack scheme to overland flow routing for high-spatial resolution distributed hydrological model. *Journal of Hydrology* **558**, 421–431. doi:10.1016/j.jhydrol.2018.01.048.

Lu, W. & Qin, X. S. 2020 Integrated framework for assessing climate change impact on extreme rainfall and the urban drainage system. *Hydrology Research* **51** (1), 77–89. doi:10.2166/nh.2019.233.

Lu, G., Liu, J., Wu, Z., Hai, H., Xu, H. & Lin, Q. 2015 Development of a large-scale routing model with scale independent by considering the damping effect of sub-basins. *Water Resources Management* **29** (14), 5237–5253. doi:10.1007/s11269-015-1115-7.

Mckay, M. D., Beckkman, R. J. & Conover, W. 2000 Comparison of three methods for selecting values of input variables in the analysis of output from a computer code. *Technometrics* **21** (2), 266–294. doi:10.2307/1271432.

Miller, J. R., Russell, G. L. & Caliri, G. 1994 Continental-scale river flow in climate models. *Journal of Climate* **7** (6), 914–928. doi:10.1175/1520-0442(1994)007<0914:CSRFIC> 2.0.CO;2.

Morisawa, M. 1958 Measurement of drainage-basin outline form. *Journal of Geology* **66** (5), 587–591. doi:10.1086/626538.

Müller Schmied, H. & Döll, P. 2017 Assessment of the terrestrial water balance using the global water availability and use model WaterGAP – status and challenges. In: *EGU General Assembly Conference*. pp. 2921.

Naden, P., Broadhurst, P., Tauveron, N. & Walker, A. 1999 River routing at the continental scale: use of globally-available data and an a priori method of parameter estimation. *Hydrology and Earth System Sciences* **3** (1), 109–123.

Nash, J. E. & Sutcliffe, J. V. 1970 River flow forecasting through conceptual models part I – a discussion of principles. *Journal of Hydrology* **10** (3), 282–290. doi:10.1016/0022-1694(70) 90255-6.

Ngongondo, C., Gong, L., Xu, C.-Y. & Alemaw, B. F. 2013 Flood frequency under changing climate in the upper Kafue River basin, southern Africa: a large scale hydrological model application. *Stochastic Environmental Research and Risk Assessment* **27** (8), 1883–1898. doi:10.1007/s00477-013-0724-z.

Olivera, F., Famiglietti, J. & Asante, K. 2000 Global-scale flow routing using a source-to-sink algorithm. *Water Resources Research* **36** (8), 2197–2207. doi:10.1029/2000WR900113.

Ragettli, S., Tong, X., Zhang, G., Wang, H., Zhang, P. & Stähli, M. 2020 Climate change impacts on summer flood frequencies in two mountainous catchments in China and Switzerland. *Hydrology Research*. In press. doi:10.2166/nh.2019.118.

Sausen, R., Schubert, S. & Dümenil, L. 1994 A model of river runoff for use in coupled atmosphere-ocean models. *Journal of Hydrology* **155** (3–4), 337–352. doi:10.1016/0022-1694(94) 90177-5.

Shepard, D. 1968 A two-dimensional interpolation function for irregularly-spaced data. In: *Proceedings of the ACM National Conference*. pp. 517–524. doi:10.1145/800186.810616.

Sircar, J. K., Ragan, R. M., Engman, E. T. & Fink, R. A. 1991 A GIS based geomorphic approach for the digital computation of time-area curves. In: *Civil Engineering Applications of*

*Remote Sensing in Water Resources Engineering* (D. B. Stafford, ed.). ASCE, New York, pp. 28–296.

Su, B. D., Jiang, T. & Jin, W. B. 2006 Recent trends in observed temperature and precipitation extremes in the Yangtze River basin, China. *Theoretical and Applied Climatology* **83** (1–4), 139–151. doi:10.1007/s00704-005-0139-y.

Tian, Z., Jing, Q., Dai, T., Jiang, D. & Cao, W. 2011 Effects of genetic improvements on grain yield and agronomic traits of winter wheat in the Yangtze River Basin of China. *Field Crops Research* **124** (3), 417–425. doi:10.1016/j.fcr.2011.07.012.

USGS 2001 *HYDRO1 k Elevation Derivative Database.* Available from: https://www.usgs.gov/centers/eros/science/usgs-eros-archive-digital-elevation-hydro1 k?qt-science_center_objects=0#qt-science_center_objects (accessed 23 November). doi:10.5066/F77P8WN0.

Wang, F., Ducharne, A., Cheruy, F., Lo, M. H. & Grandpeix, J. Y. 2018 Impact of a shallow groundwater table on the global water cycle in the IPSL land–atmosphere coupled model. *Climate Dynamics* **50** (9–10), 3502–3522. doi:10.1007/s00382-017-3820-9.

Wang, Y., Ni, J., Yue, Y., Li, J., Borthwick, A. G. L., Cai, X., Xue, A., Li, L. & Wang, G. 2019 Solving the mystery of vanishing rivers in China. *National Science Review* **6** (6), 1239–1246. doi:10.1093/nsr/nwz022.

Weisstein, E. W. *'Lambert Azimuthal Equal-Area Projection.'* From MathWorld – A Wolfram Web Resource. Available from: http://mathworld.wolfram.com/LambertAzimuthalEqual-AreaProjection.html (accessed 23 November).

Wen, Z., Xu, L. & Yang, S. 2012 A new multiscale routing framework and its evaluation for land surface modeling applications. *Water Resources Research* **48** (8), 8528. doi:10.1029/2011WR011337.

Widén-Nilsson, E., Halldin, S. & Xu, C.-Y. 2007 Global water-balance modelling with WASMOD-M: parameter estimation and regionalisation. *Journal of Hydrology* **340** (1–2), 105–118. doi:10.1016/j.jhydrol.2007.04.002.

Xu, C.-Y. 2002 WASMOD – the water and snow balance modeling system. In: *Mathematical Models of Small Watershed Hydrology Applications* (V. P. Singh & D. Frevert, eds). Water Resources Publication, Highlands Ranch, Colo, pp. 555–590.

Xu, J., Yang, D., Yi, Y., Lei, Z., Chen, J. & Yang, W. 2008 Spatial and temporal variation of runoff in the Yangtze River basin during the past 40 years. *Quaternary International* **186** (1), 32–42. doi:10.1016/j.quaint.2007.10.014.

Yang, X., Magnusson, J., Rizzi, J. & Xu, C.-Y. 2018 Runoff prediction in ungauged catchments in Norway: comparison of regionalization approaches. *Hydrology Research* **49** (2), 487–505. doi:10.2166/nh.2017.071.

Yang, X., Magnusson, J. & Xu, C.-Y. 2019 Transferability of regionalization methods under changing climate. *Journal of Hydrology* **568**, 67–81. doi:10.1016/j.jhydrol.2018.10.030.

Yang, X., Magnusson, J., Huang, S., Beldring, S. & Xu, C.-Y. 2020 Dependence of regionalization methods on the complexity of hydrological models in multiple climatic regions. *Journal of Hydrology* **582**, 124357. doi:10.1016/j.jhydrol.2019.124357.

Yao, Z., Liu, Z., Huang, H., Liu, G. & Wu, S. 2014 Statistical estimation of the impacts of glaciers and climate change on river runoff in the headwaters of the Yangtze River. *Quaternary International* **336**, 89–97. doi:10.1016/j.quaint.2013.04.026.

Zhang, Y., Min, Y., Zheng, J., Wang, G. & Niu, D. 2006 *Compilation of Flood Forecasting Plan for the Yangtze River Basin.* Hydrology Bureau of Yangtze River Water Resources Commission, Ministry of Water Resources, Wuhan (in Chinese).

Zhang, G., Xie, H., Yao, T., Li, H. & Duan, S. 2014 Quantitative water resources assessment of Qinghai Lake basin using Snowmelt Runoff Model (SRM). *Journal of Hydrology* **519**, 976–987. doi:10.1016/j.jhydrol.2014.08.022.